APPLIED SCIENCES AND ENGINEERING

3D printing of Haversian bone–mimicking scaffolds for multicellular delivery in bone regeneration

Meng Zhang[1,2], Rongcai Lin[1], Xin Wang[1,2], Jianmin Xue[1,2], Cuijun Deng[1,2], Chun Feng[1,2], Hui Zhuang[1,2], Jingge Ma[1,2], Chen Qin[1,2], Li Wan[3], Jiang Chang[1,2], Chengtie Wu[1,2]*

The integration of structure and function for tissue engineering scaffolds is of great importance in mimicking native bone tissue. However, the complexity of hierarchical structures, the requirement for mechanical properties, and the diversity of bone resident cells are the major challenges in constructing biomimetic bone tissue engineering scaffolds. Herein, a Haversian bone–mimicking scaffold with integrated hierarchical Haversian bone structure was successfully prepared via digital laser processing (DLP)–based 3D printing. The compressive strength and porosity of scaffolds could be well controlled by altering the parameters of the Haversian bone–mimicking structure. The Haversian bone–mimicking scaffolds showed great potential for multicellular delivery by inducing osteogenic, angiogenic, and neurogenic differentiation in vitro and accelerated the ingrowth of blood vessels and new bone formation in vivo. The work offers a new strategy for designing structured and functionalized biomaterials through mimicking native complex bone tissue for tissue regeneration.

INTRODUCTION

Bone tissue is an indispensable part of the human body, playing a key role in protecting internal organs and participating in human metabolism. Histologically, natural bone is composed of cortical bone at the outer layer and cancellous bone in the interior (*1*). Cortical bone is highly densified and provides the main mechanical properties of bone. In cortical bone, there are Haversian canals carrying abundant blood vessels and nerves in the longitudinal direction. The vessels in Haversian canals connect to each other through blood vessels in transversely oriented channels, which are known as Volkmann canals (*2*). Cancellous bone is a meshwork consisting of plate-like or rod-like structures at about 200-μm thickness (*3*). By one estimate, 80% of bone remodeling processes occur in cancellous bone (*4*). However, bone regeneration not only needs to reconstruct bone structure but also involves repairing other tissues like blood vessels or nerves. Osteogenesis, angiogenesis, and neurogenesis for bone regeneration are based on the interactions of multiple cells including mesenchymal stem cells (MSCs), endothelial cells (ECs), and Schwann cells (SCs) (*5*). Therefore, it is essential to meet the structural requirements and to perform the multicellular functions during the bone repairing process.

At present, the main strategies for repairing large bone defects are via autografts, allografts, and bone tissue engineering. Autografts are limited by their source and allografts face immune rejection, which limit their further application. Bone tissue engineering, however, has become an efficient approach for bone repair. Although many bone tissue engineering scaffolds have been developed, most of the prepared scaffolds are simple structures, which can not be used for achieving the spatial arrangement of multiple cells. However, a crucial aspect of mimicking tissue is modulating the cellular processes such as cell distributions and multicellular interactions in the specific three-dimensional (3D) structure (*6*). Consequently, fabrication of bone tissue engineering scaffolds with multicellular delivery and complex morphologies akin to native bone tissue remains challenging for bone tissue regeneration (*7*).

Recently, biomimetic strategies have attracted much attention in constructing high-performance bone tissue engineering biomaterials. Many approaches, such as freeze casting (*8*), layer-by-layer assemble (*9*), and 3D printing (*10*), have been used to fabricate biomimetic biomaterials. Among these methods, 3D printing offers the prospect of fabricating materials with specific customized structures similar to native tissue (*11*). Our group has previously prepared the lotus root–like scaffolds for the regeneration of vascularized bone tissue (*12*) and hot dog–like scaffolds by 3D printing for drug delivery to further promote bone regeneration (*13*). 3D printing has even been used to prepare complicated artificial heart (*14*) and lung tissues (*15*). Constructing biomaterials with hierarchical bone-mimicking structure using 3D printing technology provides multicellular delivery and, thus, promote the vascularization and neurotization in bone regeneration.

Herein, inspired by the hierarchical structure and functions of bone, Haversian bone–mimicking bioceramic scaffolds were successfully fabricated by digital laser processing (DLP)–based 3D printing technology. The method provided a fast, high-precision, and robust strategy to fabricate structurally diversified bioceramic scaffolds from a single precursor slurry by a one-step process. The Haversian bone–mimicking structure composed of cortical bone structure (containing Haversian canals and Volkmann canals) and cancellous bone structure could be easily controlled by the custom design. The multicellular delivery system with MSCs transported by the cancellous bone structure and ECs/SCs transported by the Haversian canals represented a simple but versatile design. The Haversian bone–mimicking scaffold–based multicellular delivery system exhibited notably improved osteogenic and angiogenic effects as compared with the unicellular delivery system both in vitro and in vivo. Thus, we proposed a concept of 3D structure–based coculture platform and developed a Haversian bone–mimicking scaffold–based multicellular delivery system with osteogenic cells and angiogenic/neurogenic cells distributed at the specific location for active bone tissue engineering.

[1]State Key Laboratory of High Performance Ceramics and Superfine Microstructure, Shanghai Institute of Ceramics, Chinese Academy of Sciences, Shanghai 200050, P. R. China. [2]Center of Materials Science and Optoelectronics Engineering, University of Chinese Academy of Sciences, Beijing 100049, P. R. China. [3]Beijing Ten Dimensions Technology Co., Ltd., Beijing 100084, P. R. China.
*Corresponding author. Email: chengtiewu@mail.sic.ac.cn

RESULTS

Design and fabrication of Haversian bone–mimicking scaffolds

To replicate the bone structure and reconstruct the cellular components, Haversian bone–mimicking scaffolds with Haversian canals, Volkmann canals, and cancellous bone structure were fabricated for delivery of osteogenic and angiogenic cells (Fig. 1). Akermanite bioceramic materials were used here due to their excellent osteoconductivity and osteoinductivity for bone regeneration. Five kinds of Haversian bone–mimicking scaffolds with different numbers and diameters of Haversian canals were successfully fabricated by DLP-based 3D printing technology (Fig. 2, A to E). Haversian canals (magenta arrows) were tubular channels arranged at the peripheral part of the scaffolds oriented at an angle of 20° to the vertical direction. The diameter of the Haversian canals could be changed to 0.8 mm (Fig. 2F), 1.2 mm (Fig. 2G), and 1.6 mm (Fig. 2H). Volkmann canals were annular channels connecting the Haversian canals oriented at the horizontal direction (Fig. 2F, a to e, blue arrows). The diameter of the Volkmann canals was set as 0.8 mm, which was optimized according to the printing resolution and postprocessing. As the Haversian canals were interconnected, one of the Haversian canals was substituted as a 1.6-mm-diameter one for routine cell seeding. Cancellous bone was designed as meshwork within the cylindrical hole in the central part of the scaffolds (Fig. 2I). Three cuboids on the same horizontal plane were duplicated and rotated at 45° in the vertical direction to obtain the meshwork. Interconnected Haversian canals were isolated from the cancellous bone structure for noncontact cell coculture. Furthermore, the periphery and bottom of the scaffolds were sealed so that the scaffolds could be used for holding the seeded cells (movie S1). In the microscopic view, bioceramic scaffolds were well sintered to enhance the mechanical properties (Fig. 2J). The surface roughness of the cancellous and cortical bone structures were 12.52 ± 9.17 and 18.90 ± 17.86 μm, respectively (fig. S1). Thus, Haversian bone–mimicking scaffolds with versatile morphologies were successfully fabricated by DLP-based 3D printing technology.

Tunable mechanical property and porosity of Haversian bone–mimicking scaffolds

To investigate the relationship among morphology, mechanical property, and porosity, scaffolds with a diameter of 10 mm and height of 11 mm were designed with different numbers of Haversian canals (movie S2), diameters of Haversian canals (movie S3), and numbers of Volkmann canals (movie S4). To explore the influence of the number of Haversian canals on mechanical property and porosity, the numbers of Haversian canals of scaffolds were designed as 2, 4, and 8, respectively (Fig. 3, A to C). With the increasing number of Haversian canals, the compressive strength of scaffolds decreased (Fig. 3D), while the porosity of scaffolds was increased (Fig. 3E). Furthermore, scaffolds with different diameters of Haversian canals were prepared to further investigate their porosity and strength. For the groups in which the number of Haversian canals was 8, the diameter of Haversian canals could be changed to 0.8, 1.2, and 1.6 mm, respectively (Fig. 3, F to H). As the diameter of Haversian canals increased, the compressive strength was first enhanced and then reduced (Fig. 3I) while the porosity increased (Fig. 3J). Furthermore, the number of Volkmann canals was allowed to be changed to 0, 1, 2, and 3 (Fig. 3, K to N). It was found that the compressive strength of the scaffolds decreased (Fig. 3O) while the porosity increased (Fig. 3P) with the increasing number of Volkmann canals, indicating that radial channels did not contribute to axial load. The compressive modulus also decreased with the increasing number of Volkmann canals (fig. S2). To investigate the flexural strength, scaffolds with the diameter of 10 mm and height of 25 mm were designed (fig. S3A). The flexural strength of scaffolds increased with the increasing number of Haversian canals, increasing diameter of Haversian canals, and decreasing number of Volkmann canals (fig. S3, B to D). Thus, a range of 9.67 to 26.72 MPa for compressive strength, 15.21 to 21.12 MPa for flexural strength, and 22.0 to 40.3% for porosity of the scaffolds could be well controlled by modulating the number of Haversian canals, the diameter of Haversian canals, and the number of Volkmann canals.

Coculture of osteogenic and angiogenic cells in Haversian bone–mimicking scaffolds

Vascularization is a key process in bone remodeling. To investigate the cellular interactions in the osteogenesis and angiogenesis processes, five kinds of scaffolds with different numbers and diameters of Haversian canals as shown in Fig. 2 were used for delivery of coculture cells. Human bone marrow stem cells (HBMSCs) and human umbilical vein endothelial cells (HUVECs) were seeded separately with the ratio of 1:1. The 1:1 ratio was chosen because it was demonstrated that the expression of angiogenic genes and proliferation were highest when the MSC:EC ratio was 1:1 (*16*). Confocal laser scanning microscopy (CLSM) and scanning electron microscopy (SEM) images showed the morphology of HBMSCs and HUVECs in coculture models in Haversian bone–mimicking scaffolds. HBMSCs seeded in cancellous bone structure extended well and exhibited numerous filopodia (Fig. 4, A and E). HUVECs seeded on Haversian canals with different diameters permeated through the Haversian canals (Fig. 4, B to D and F to H). The separated CLSM images of cells stained with phalloidin and 4′,6-diamidino-2-phenylindole (DAPI) are shown in fig. S4. The cell proliferation test was performed. It was verified that the coculture group outperformed the HBMSC and HUVEC monoculture group in all five kinds of scaffolds (Fig. 4, I and J). Among the five kinds of scaffolds, the coculture group containing Haversian canals with the diameter of 1.2 mm and number of 8 was selected for analysis of gene expression due to its good performance in mechanical testing and cell proliferation. The individual cell proliferation of HBMSCs and HUVECs cultured with the extracts from the Haversian bone–mimicking bioceramic scaffolds on days 1, 3, and 7 was also investigated. The extracts from the scaffolds showed no toxicity for 1 and 3 days (fig. S5). To explore the individual gene expression level of HBMSCs and HUVECs in the coculture group, the coculture cells were separated as Co-HBMSC (HBMSCs in coculture group) and Co-HUVEC (HUVECs in coculture group) using magnetic beads. Osteogenic and angiogenic gene expression levels of HBMSCs, HUVECs, Co-HBMSC, and Co-HUVEC were analyzed. On day 3, the expression of BMP2 in Co-HUVEC was significantly higher than that in HUVEC monoculture. Moreover, Co-HBMSC revealed higher gene expression levels of Col1 and ALP than the HBMSC monoculture (Fig. 4K). Then, the expression of angiogenic gene markers kinase domain receptor (KDR), endothelial NO synthase (eNOS), and vascular endothelial cadherin (VE-cadherin) was investigated (Fig. 4L). The results showed that Co-HUVEC expressed a higher level of these markers than that of the HUVEC monoculture. The effects of different diameters and numbers of Haversian canals on the osteogenic and angiogenic gene expression of cocultured HBMSC-HUVEC seeded on scaffolds were

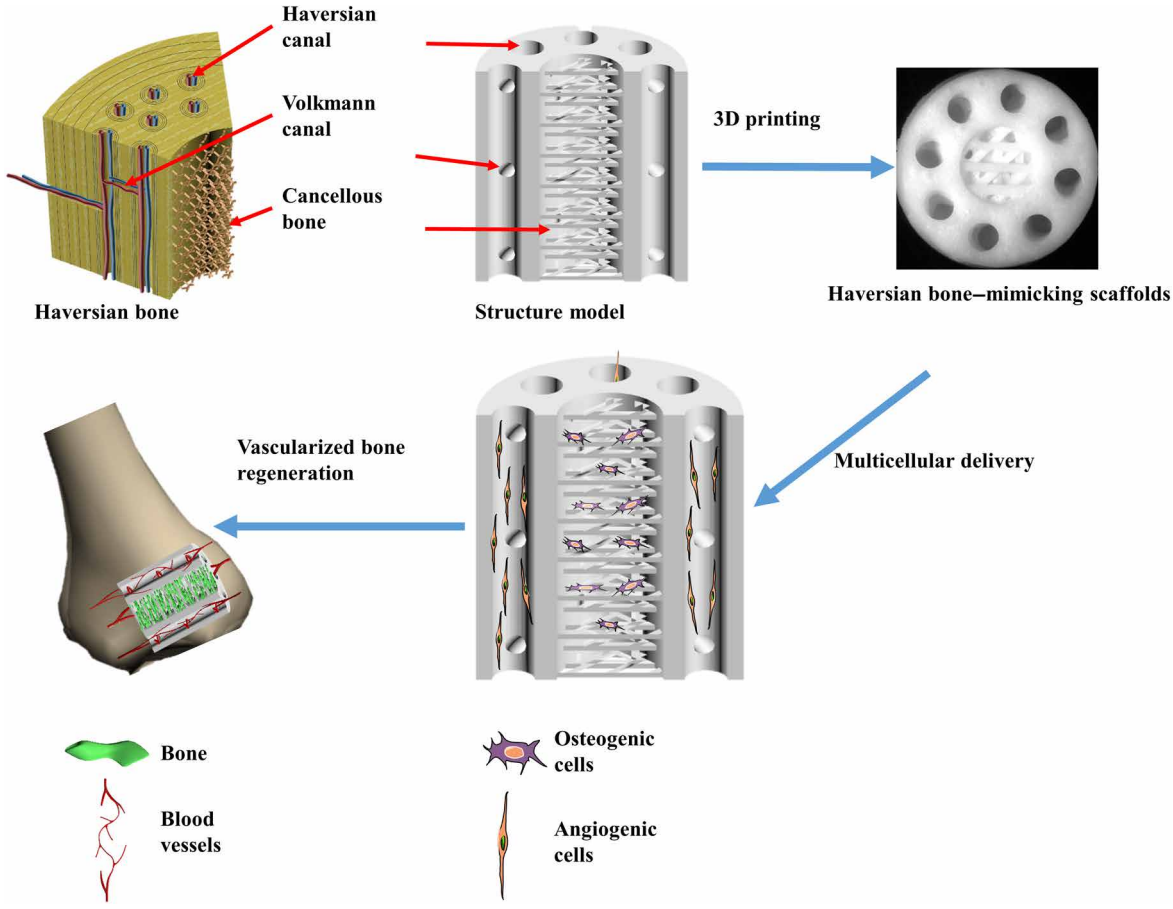

Fig. 1. 3D printing Haversian bone–mimicking scaffolds integrated with Haversian canals, Volkmann canals, and cancellous bone structure for delivery of osteogenic and angiogenic cells. Osteogenic cells were seeded in cancellous bone structure of scaffolds, and angiogenic cells were seeded on Haversian canals. The Haversian bone–mimicking structure–based multicellular delivery system contributed to the formation of new bone and new blood vessels.

investigated. For different diameters of Haversian canals, the group with the diameter of 1.6 mm performed the best in both the osteogenic and angiogenic gene expression (fig. S6).

Coculture of osteogenic and neurogenic cells in Haversian bone–mimicking scaffolds

To demonstrate the universality of our scaffolds for establishing a resident bone cell coculture system, an rBMSC (rat bone marrow–derived MSC)–rSC (rat SCs) coculture system was developed. Five groups with different ratios of rBMSCs:rSCs (rBMSC monoculture, rSC monoculture, 3:7, 5:5, 7:3) were investigated. As nerves ran parallel with vessels through Haversian canals, rSCs were seeded on Haversian canals cocultured with rBMSCs seeded in the cancellous bone structure. CLSM images showed that rBMSCs in the rBMSC monoculture (Fig. 5A) and rBMSC-rSC coculture groups (Fig. 5, B to D) exhibited proper adhesive abilities in cancellous bone structure at day 1, and the cell density increased as the proportion of rBMSCs was enhanced. The separated CLSM images of cells stained with phalloidin and DAPI are shown in fig. S7. Moreover, rSCs in the rSC monoculture (Fig. 5E) and rBMSC-rSC coculture groups (Fig. 5, F to H) penetrated through the Haversian canals at day 1, and the cell density decreased as the proportion of rSCs was reduced. The proliferation of the coculture groups was obviously promoted compared with the rBMSC monoculture group at days 1, 3, 7, and 14. At day 7, the 3:7 and 5:5 groups exhibited better proliferative activities than both the rBMSC monoculture group and the rSC monoculture group (Fig. 5I). For the different coculture groups, the proliferative activity was enhanced as the proportion of rSCs increased, which might be due to the great difference of proliferation rate between rBMSCs and rSCs. The individual cell proliferation of rBMSCs and rSCs cultured with the extracts from the Haversian bone–mimicking bioceramic scaffolds on days 1, 3, and 7 was also investigated. The extracts from the scaffolds showed no toxicity for 1 and 3 days (fig. S8). To further explore the cellular interactions between rBMSCs and rSCs, neurogenic gene expression at day 3 was then evaluated through real-time polymerase chain reaction (RT-PCR) (Fig. 5J). Nerve growth factor (NGF), high-affinity NGF receptor (TrkA), brain-derived neurotrophic factor (BDNF), and SC marker S100 were selected to investigate the neurogenesis of the rBMSC-rSC coculture system. The gene expression levels of NGF, TrkA, and BDNF in the coculture groups were higher than those in both monoculture groups, indicating a synergistic effect in the potential of axonal regeneration. However, the S100 expression level of the coculture groups was lower than that of the rBMSC group but higher than that of the rSC group, which exhibited an additive effect on the differentiation potential toward Schwann-like cells. The

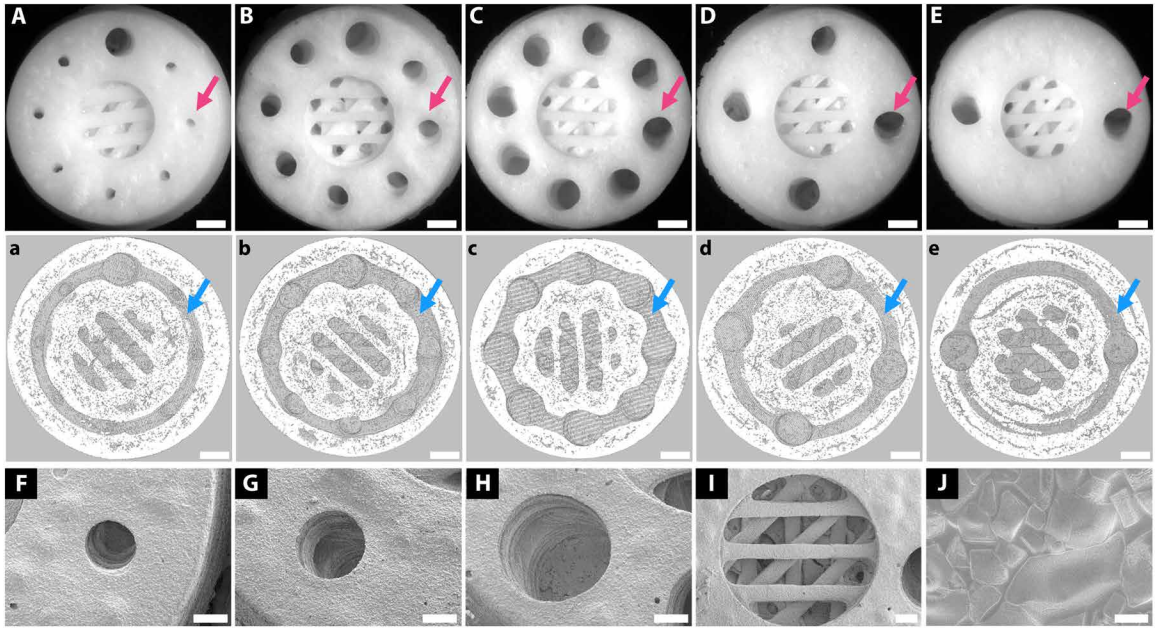

Fig. 2. 3D printing of Haversian bone–mimicking bioceramic scaffolds with cortical bone and cancellous bone structure. Cortical bone structure contained Haversian canals and Volkmann canals. (**A** to **E**) Optical microscope images exhibited different diameters (*D*) and numbers (*N*) of Haversian canal indicated by magenta arrows (A) $N = 8$, $D = 0.8$ mm; (B) $N = 8$, $D = 1.2$ mm; (C) $N = 8$, $D = 1.6$ mm; (D) $N = 4$, $D = 1.6$ mm; and (E) $N = 2$, $D = 1.6$ mm. Scale bars, 1 mm. (**a** to **e**) Micro–computed tomography (CT) images show Volkmann canals (blue arrows) connecting Haversian canals in the interior of scaffolds. Scale bars, 1 mm. (**F** to **J**) SEM images presented the microstructure of the scaffolds. Haversian canal on the periphery of scaffolds with different diameters of (F) 0.8 mm, (G) 1.2 mm, and (H) 1.6 mm. Scale bars, 400 μm. (**I**) Cancellous bone structure in the center of the scaffolds. Scale bar, 400 μm. (**J**) Microstructure at the surface showed a well-sintered scaffold. Scale bar, 6 μm.

effects of different diameters and numbers of Haversian canals on the neurogenic gene expression of cocultured rBMSC-rSC seeded on scaffolds were investigated (fig. S9). For different diameters of Haversian canals, the group with the diameter of 1.2 mm performed better in the NGF and TrkA expression, and the group with the diameter of 0.8 mm performed better in the S100 expression.

In vivo osteogenesis and angiogenesis of Haversian bone–mimicking scaffold–based coculture system

To further verify the osteogenesis and angiogenesis of the scaffold-based coculture system in vivo, a rabbit bone marrow–derived MSC–rabbit aortic EC (RBMSC-RAEC) coculture system was established for repairing femoral defects of rabbits. Five groups with different culture modes were investigated: blank, AKT, RBMSC, RAEC, and coculture. After 8 weeks of implantation, animals were euthanized followed by perfusion of Microfil, and the samples were harvested (Fig. 6, A to E). Micro–computed tomography (CT) images showed the newly formed bone (green) within scaffolds (red) in the transversal section (Fig. 6, F to J) and longitudinal section (Fig. 6, f to j). More newly formed bone was found in the coculture group than in the monoculture groups and the cell-free scaffold (AKT) group. Statistical analysis demonstrated that the bone volume/total volume (BV/TV) value of the coculture group was significantly higher than that of the monoculture groups and the cell-free scaffold group, which verified the osteogenic ability of the scaffold-based coculture system (Fig. 6P). Histological analysis showed that more new blood vessels (blue) and new bone (red) formed in the coculture group than that in the monoculture groups and the cell-free scaffold group (Fig. 6, K to o, and fig. S10). Furthermore, quantitative analysis showed that the new vessel density of the coculture group was significantly higher than that of the monoculture groups and the cell-free scaffold group, indicating the improved angiogenic activity of the scaffold-based coculture system (Fig. 6Q).

DISCUSSION

Generally, mimicking the structural and biological features of bone tissue usually required multiple approaches. For example, electrospinning combined with twin screw extrusion was used for fabricating core-shell scaffolds by mimicking the osteon-like structures (*17*). Other methods, such as modular tissue engineering, always required special molds to construct osteon-like structures (*18*). The operational complexity of these approaches makes it impossible to prepare osteon-like biomaterials efficiently and accurately. At present, 3D printing is an advanced method for manufacturing complex structures by one-step approach without any templates. For instance, extrusion-based 3D printing was used to fabricate biphasic osteon-like scaffolds with a concentric triple-ring structure (*19*). However, the prepared osteon-like scaffolds based on the concentric tubes could not mimic the interconnected Haversian canals and Volkmann canals in cortical bone. Compared with traditional extrusion-based 3D printing, DLP-based 3D printing provided a more versatile strategy to integrate various microstructures into one model (*20*). Previous studies demonstrated cortical bone-mimicking scaffolds without cancellous bone structure via DLP-based 3D printing (*21*). However, besides cancellous bone structure, the biological functions of these structures, the key points of tissue reconstruction in vivo, were neglected (*22*). Thus, a simple model mimicking the primary structure and function of Haversian bone is necessary.

Here, we designed a series of Haversian bone–mimicking scaffolds with integrated hierarchical structures (including Haversian canals,

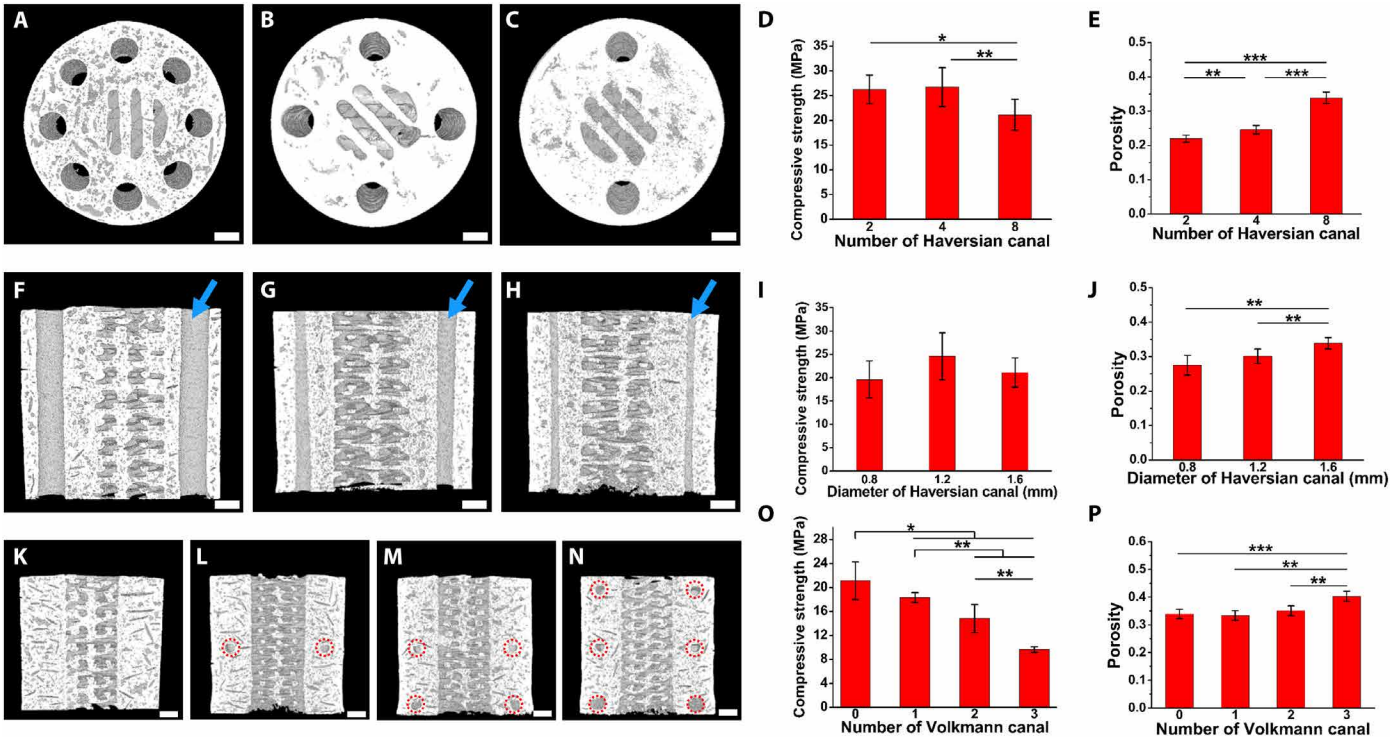

Fig. 3. Characterization of Haversian bone–mimicking bioceramic scaffolds. (**A** to **C**) Micro-CT images of scaffolds with different numbers of Haversian canals, (A) $N = 8$, (B) $N = 4$, and (C) $N = 2$. (**D**) Compressive strength of scaffolds with different numbers of Haversian canals. (**E**) Porosity of scaffolds with different numbers of Haversian canals. (**F** to **H**) Micro-CT images of scaffolds with different diameters of Haversian canals indicated by blue arrows, (F) $D = 1.6$ mm, (G) $D = 1.2$ mm, and (H) $D = 0.8$ mm. (**I**) Compressive strength of scaffolds with different diameters of Haversian canals. (**J**) Porosity of scaffolds with different diameters of Haversian canals. (**K** to **N**) Micro-CT images of scaffolds with different numbers of Volkmann canals indicated by red circles for (K) $N = 0$, (L) $N = 1$, (M) $N = 2$, and (N) $N = 3$. (**O**) Compressive strength of scaffolds with different numbers of Volkmann canals. (**P**) Porosity of scaffolds with different numbers of Volkmann canals. $n = 6$ replicates. $^*P < 0.05$, $^{**}P < 0.01$, $^{***}P < 0.001$. Scale bars, 1 mm.

Volkmann canals, and cancellous bone) and investigated the biological functions of these structures by establishing a multicellular delivery system. The scaffolds with integrated hierarchical Haversian bone structures were fabricated via simple template-free DLP-based 3D printing, and the structure parameters were precisely tunable in the 3D modeling software. The versatility of our design was demonstrated through integrating three various structures into one scaffold, which is challenging for other fabrication methods. Furthermore, our method was advanced in manufacturing bioceramic scaffolds, which were too brittle to be fabricated into complex structures.

As bone structures and strength vary among patients, ages, and diseases, it is necessary to prepare Haversian bone–mimicking scaffolds with controlled strength (*23*). The strength of long bone depended on cortical bone (*24*), and the porosity of cortical bone was a considerable feature of bone quality (*25*). Therefore, we set out to alter the parameters of the cortical bone structure and demonstrated that the compressive strength and the porosity of Haversian bone–mimicking scaffolds were precisely tunable by altering the parameters of Haversian bone–mimicking structures. On the one hand, increasing the number of Haversian and Volkmann canals led to more channels in the longitudinal and transverse directions, respectively, while increasing the diameter of Haversian canals enlarged the volume of channels. On the other hand, we suggested that Haversian canals could disperse the compressive and the flexural stress, which prevented the exceedingly early failure due to the local fracture (*26*). The modification of these parameters contributed to the regulation of porosity and, thus, led to the alteration of compressive and flexural strength. Here, a range of 9.67 to 26.72 MPa for compressive strength and a range of 15.21 to 21.12 MPa for flexural strength could be obtained by controlling the number of Haversian canals, the diameter of Haversian canals, and the number of Volkmann canals, which provided a guide for optimization design of scaffolds with various strengths according to requirements of different patients.

Conventional 2D coculture system could not replicate the 3D environment in vivo, and many approaches for 3D coculture were developed (*27*). The Transwell method provided a simple model to culture different types of cells in a noncontact way for routine use. Microfluidic devices or scaffolds realized the exact control of cell distribution and quantity (*28*). However, these systems were not adaptive for implantation in bone tissue. Tissue engineering scaffolds provided a 3D environment for cell coculture and met the need of mechanical strength. For example, cocultured cells were mixed on the scaffolds in a tricalcium phosphate (β-TCP) scaffold-based HBMSC-HUVEC coculture system (*29*). However, the coculture method by mixing various types of cells failed to control the spatial distribution of different cells. Furthermore, it was difficult to identify whether the cocultured cells interacted by direct contact or paracrine effects. Our Haversian bone–mimicking scaffold–based noncontact coculture system was successfully constructed to achieve the multicellular spatial distribution, mimicking the natural bone and tissue cells.

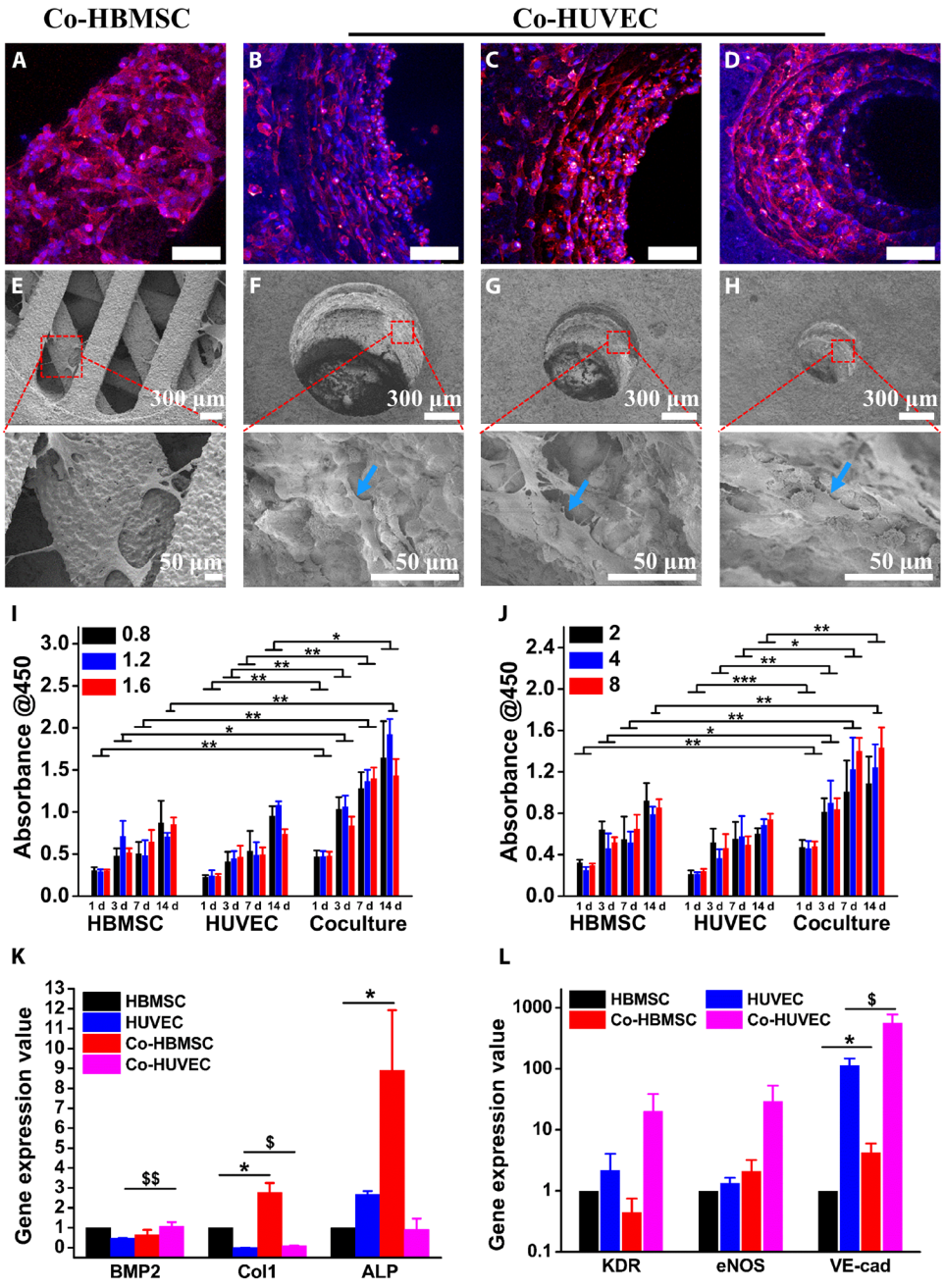

Fig. 4. Haversian bone–mimicking bioceramic scaffolds for the HBMSC-HUVEC coculture system performed better in cell proliferation and angiogenic differentiation than monoculture. (**A** to **D**) CLSM images of HBMSCs seeded on the cancellous bone structure (A) and HUVECs seeded on the Haversian canal with different diameters, (B) $D = 1.6$ mm, (C) $D = 1.2$ mm, and (*D*) D = 0.8 mm. Scale bars, 100 μm. (**E** to **H**) SEM images of (E) HBMSCs seeded on the cancellous bone structure and HUVECs seeded on the Haversian canal with different diameters of (F) 1.6 mm, (G) 1.2 mm, and (H) 0.8 mm. (**I** and **J**) The proliferation activity of HBMSC, HUVEC, and cocultured HBMSC-HUVEC seeded on scaffolds with different (I) diameters and (J) numbers of Haversian canals after culturing for 1, 3, 7, and 14 days. $n = 6$ replicates. (**K** and **L**) The osteogenic (K) and angiogenic (L) gene expression of HBMSC, HUVEC, Co-HBMSC (HBMSCs in HBMSC-HUVEC coculture), and Co-HUVEC (HUVECs in HBMSC-HUVEC coculture) for 3 days. $n = 3$ replicates. $^{*}P < 0.05$, $^{**}P < 0.01$, $^{***}P < 0.001$, $^{\$}P < 0.05$, $^{\$\$}P < 0.01$.

Benefiting from the hierarchical structure of scaffolds, we successfully constructed the Haversian bone–mimicking scaffold–based HBMSC-HUVEC coculture system, in which HBMSCs grew in cancellous structure of scaffolds and HUVECs grew on Haversian canals. Our findings revealed that the coculture cells showed normal cell morphologies and a higher proliferation rate compared with monoculture cells at days 1, 3, 7, and 14 regardless of the number and diameter of Haversian canals of scaffolds. Previous studies demonstrated that the proliferation of HBMSC-HUVEC contact coculture cells on the β-TCP scaffolds was in proportion to the ratio and proliferation rate of HBMSCs and HUVECs. Moreover, HBMSCs might inhibit the expansion of HUVECs due to their high proliferation rate (*30*).

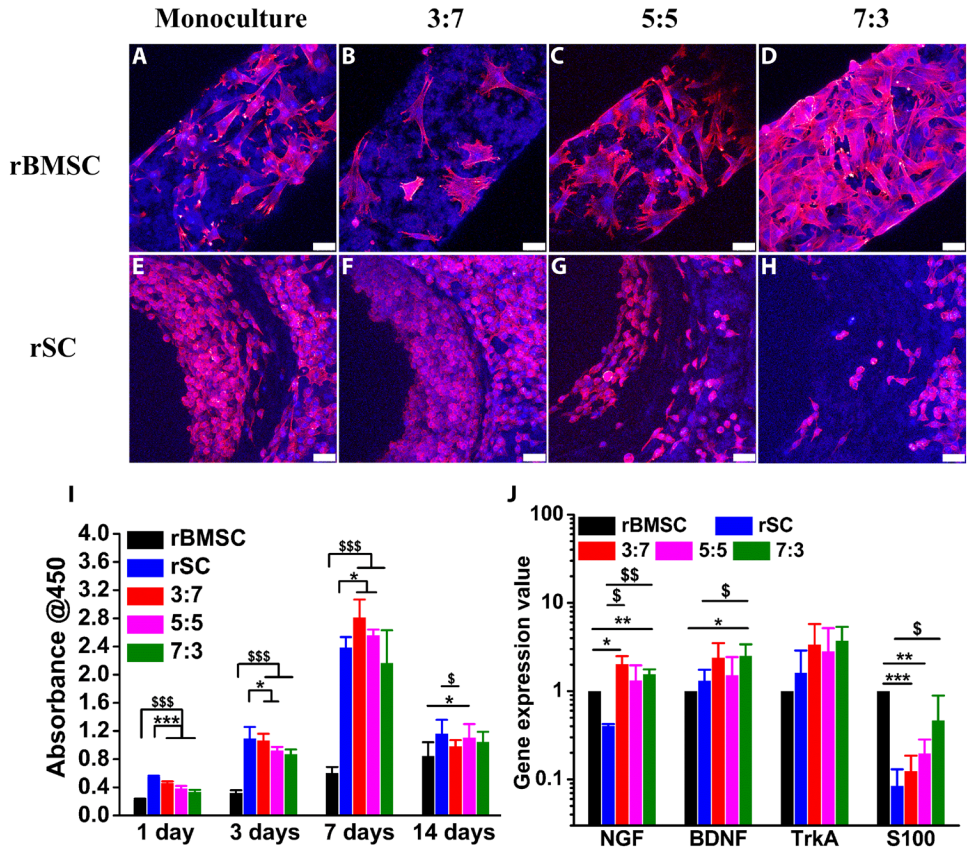

Fig. 5. Haversian bone–mimicking bioceramic scaffold–based rBMSC-rSC coculture system performed better in cell proliferation and neurogenic differentiation than monoculture. (**A** to **D**) The CLSM images of rBMSC in the (A) rBMSC monoculture group and rBMSC-rSC coculture group with the ratio of rBMSC to rSC being (B) 3:7, (C) 5:5, and (D) 7:3 seeded on the cancellous bone of scaffolds. Scale bars, 50 μm. (**E** to **H**) The CLSM images of rSCs in (E) the rSC monoculture group and rBMSC-rSC coculture group with the ratio of rBMSCs to rSCs being (F) 3:7, (G) 5:5, and (H) 7:3 seeded on the Haversian canal of scaffolds. Scale bars, 50 μm. (**I**) The proliferation of rBMSC, rSC, and rBMSC-rSC coculture with different ratio of rBMSCs to rSCs. $n = 6$ replicates. (**J**) The neurogenic genes expression of rBMSC, rSC, and rBMSC-rSC coculture with different ratio of rBMSCs to rSCs for 3 days. $n = 3$ replicates. $^{*}P < 0.05$, $^{**}P < 0.01$, $^{***}P < 0.001$, $^{\$}P < 0.05$, $^{\$\$}P < 0.01$, $^{\$\$\$}P < 0.001$.

It was also found that MSC-EC contact coculture decreased the proliferation of ECs (*31*). However, our results suggested that the Haversian bone–mimicking scaffolds provided more appropriate 3D structure for cell distribution and proliferation. Furthermore, ALP, Col1 in Co-HBMSC and BMP2, KDR, and VE-cadherin in Co-HUVEC were significantly higher than that in monoculture. BMP2 was known as an early marker of bone formation and served as a signaling molecule facilitating the expression of ALP. ALP and Col1 were the early and late markers of osteogenesis, respectively (*32*). The enhanced expression level of ALP and Col1 indicated more bone ECM (extracellular matrix) synthesis and more remarkable osteogenic differentiation effect toward osteoblasts. Simultaneously, the up-regulation of VE-cadherin (a junctional protein) suggested that HBMSCs regulated HUVEC junctions through paracrine effects. One possible reason of the improvement of the gene expression was that the activation of KDR was followed by the expression of BMP2 and the activation of eNOS, which initiated osteogenic differentiation and angiogenic differentiation through facilitating ALP expression and nitric oxide production, respectively (*33*). Furthermore, the osteogenic and angiogenic gene expression of cocultured HBMSC-HUVEC seeded on scaffolds increased with the increasing diameter of Haversian canals. It is likely that the Haversian canals with a diameter of 1.6 mm were advantageous to the delivery of nutrition, which constructed the more proper microenvironment to promote the osteogenic and angiogenic differentiation of the coculture cells. Therefore, the Haversian bone–mimicking scaffold–based noncontact coculture system had distinct advantages for spatial distribution of different cells, which further promoted their proliferation and differentiation.

Besides blood vessels, bone also contains a wealth of sensory nerves, which are important for bone formation and remodeling (*34*). Here, we further established the Haversian bone–mimicking scaffold–based rBMSC-rSC coculture system with rBMSCs grown in cancellous bone structure and rSCs grown on Haversian canals. Our results indicated that the rBMSC-rSC coculture system exhibited a better proliferation and a higher expression of NGF, BDNF, TrkA, and S100 as compared to rSC monoculture. It was found that BMSCs could promote SC proliferation and were traditionally used to facilitate the recovery of sensory system (*35*). Our results were in accordance with the previous study that rat MSCs promoted the proliferation and expression of neurotrophic factors or their receptors of SCs in the noncontact coculture of MSCs and SCs by the Transwell method (*36*). However, the effect of scaffold parameters on the neurogenic differentiation of the cocultured rBMSCs and rSCs was not significant. Vascularization and neurotization are important features in bone, whereas it is difficult to construct a neurovascularized

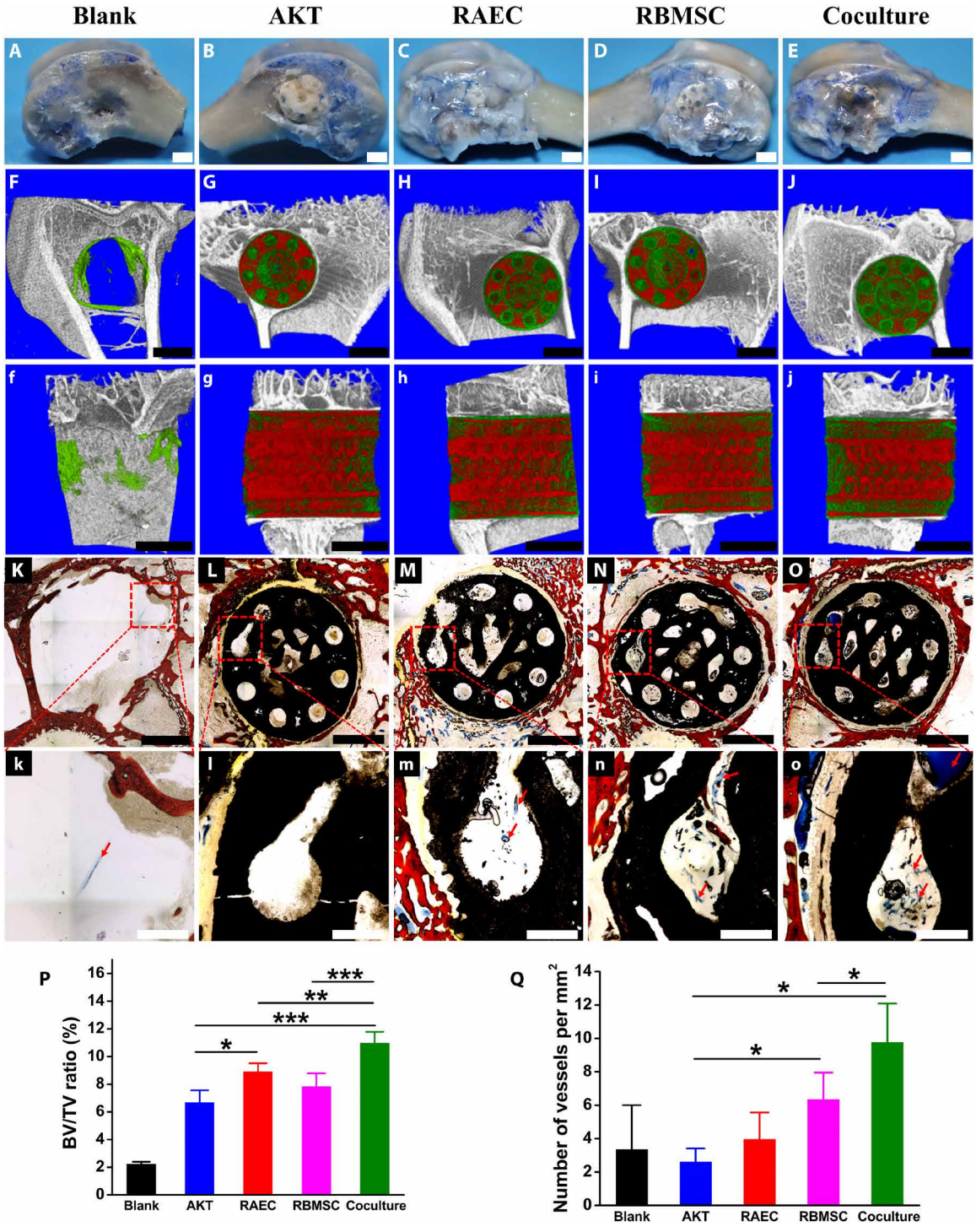

Fig. 6. The Haversian bone–mimicking bioceramic scaffold–based RBMSC-RAEC coculture system enhanced the formation of new bone and new blood vessels in rabbit femoral defects. (**A** to **E**) Digital photographs showed the defects in the (A) blank group and scaffolds implanted into the defect (B) cell-free AKT scaffold group, (C) RAEC monoculture group, (D) RBMSC monoculture group, and (E) RBMSC-RAEC coculture group perfused with Microfil (blue). Scale bars, 3 mm. (**F** to **j**) Micro-CT images exhibited (F to J) sagittal view and (f to j) transverse view of the five groups at week 8, respectively (green for newly formed bone and red for scaffolds). Scale bars, 3 mm. (**K** to **O**) The sections from Microfil-perfused samples stained with picric acid-acid fuchsin. Scale bars, 2 mm. (**k** to **o**) Magnified images of the marked area in (K to O). Scale bars, 500 μm. The red arrows indicated blood vessels (blue). (**P**) The volume ratio of the newly formed bone to defects (BV/TV) of all groups. $n = 4$ replicates. (**Q**) The density of newly formed vessels of all groups. $n = 3$ replicates. $^{*}P < 0.05$, $^{**}P < 0.01$, $^{***}P < 0.001$. (Photo credit: Meng Zhang, State Key Laboratory of High Performance Ceramics and Superfine Microstructure, Shanghai Institute of Ceramics, Chinese Academy of Sciences, Shanghai 200050, P. R. China. Center of Materials Science and Optoelectronics Engineering, University of Chinese Academy of Sciences, Beijing 100049, P. R. China.)

scaffold due to the complexity of regulating different cell types (*37*, *38*). Our work provided a coculture method to arrange the spatial distribution of different cell types in a Haversian bone–mimicking scaffold and demonstrated the angiogenic and neurogenic potential of the Haversian bone–mimicking scaffold-based coculture systems due to the interactions between different types of cells.

In vivo rabbit femoral defect experiment further demonstrated that more new bone and blood vessels formed in Haversian canals in the RBMSC-RAEC coculture group as compared to the monoculture groups and the cell-free scaffold group. The BV/TV ratio of the cell-free scaffold group was significantly higher than that of the blank group, suggesting that the Haversian bone–mimicking scaffolds were conducive to the early bone formation. Furthermore, the RAECs distributed on the Haversian canals and RBMSCs distributed in the cancellous bone structure also played important roles in accelerating the blood vessel ingrowth and new bone formation. It was likely that the coculture cells secreted more osteogenic and angiogenic factors, which participated in the mineralization process and the vessel formation and further facilitated the angiogenesis and osteogenesis. Moreover, the cocultured RBMSCs and RAECs might secrete more ECM, which provided a physiological environment for cell proliferation, migration, and differentiation.

Considering the clinical applications of Haversian bone–mimicking scaffolds, there are still some issues to be studied. First of all, more bone-resident cells such as osteoblasts, osteoclasts, and macrophages should be further considered in the coculture system. The mechanism of multicellular synergistic effects is not fully understood. Further studies are needed to identify the individual effects of coculture cells on the formation of new bone, blood vessels, and nerves in the Haversian bone–mimicking scaffold–based coculture system.

In summary, we successfully prepared Haversian bone–mimicking scaffolds with Haversian canals, Volkmann canals, and cancellous bone structure through DLP-based 3D printing technology. The Haversian bone–mimicking scaffolds exhibited tunable mechanical property and porosity by altering the structure parameters according to the custom design. In addition, the Haversian bone–mimicking scaffolds were effective in delivering osteogenic cells, angiogenic cells, and neurogenic cells, which exhibited favorable osteogenesis and angiogenesis both in vitro and in vivo. This work proposed a biomimetic strategy for designing structured and functionalized biomaterials for tissue regeneration.

MATERIALS AND METHODS

Material preparation

Fifty grams of AKT ($Ca_2MgSi_2O_7$, HQ-Ar-Q, Kunshan Chinese Technology New Materials Co. Ltd., Kunshan, Jiangsu, China) bioceramic powder and 1.25 g of 45S5 bioactive glass (Kunshan Chinese Technology New Materials Co. Ltd., Kunshan, Jiangsu, China) powder were ball milled with 50 g of photosensitive resin (WANHAO Co. Ltd., Jinhua, Zhejiang, China) to obtain the precursor slurry.

Scaffold fabrication

3D structures of Haversian bone–mimicking scaffolds were designed by 3ds Max (Autodesk) to obtain stereolithography (STL) files. The precursor slurry was polymerized and cross-linked by a DLP-based 3D printer (AUTOCERA-M, Beijing Ten Dimensions Technology Co. Ltd., China) following STL files. The exposure time is 3 s for each slice 50 μm thick. The wavelength of the light source is 405 nm. After printing, the samples were detached from the prototyping platform and washed in alcohol via ultrasonic cleaning for 30 s to remove the uncured resin. The green bodies of the scaffolds were then sintered at 1350°C for 3 hours at a heating rate of 2°C/min to obtain the pure bioceramic scaffolds.

Material characterization

The macroscopic morphology at the surface of the Haversian bone–mimicking scaffolds was characterized by optical microscopy (S6D, Leica, Germany). The internal structure of the scaffolds was reconstructed by micro-CT (SKYSCAN1172, Bruker, Germany). The microstructure of the scaffolds was observed by SEM (S-4800, Hitachi, Japan). Compressive and flexural strength tests were performed by the universal testing machine (AG-I, Shimadzu, Japan) on cylindrical scaffolds (Φ7.7 mm by 8.5 mm for compressive strength tests and Φ7.7 mm by 17 mm for three-point bending tests). The compressive modulus was defined as the slope of the initial linear regions of the stress-strain curves. The porosity of the scaffolds was investigated by the Archimedes' method as described previously (*12*). The surface roughness of the scaffolds was measured with a contact surface profilometer (Daktak-XT, Bruker, Germany) at a speed of 0.05 mm/s and a scanning length of 1 mm.

Cell culture

HBMSCs (Cyagen, Guangzhou, China) were cultured in HBMSC culture medium (Cyagen, Guangzhou, China). HUVECS were isolated by a previously described method (*39*). HUVECS were cultured in EC medium (Sciencell, America). rBMSCs (Cyagen, Guangzhou, China) were cultured in rBMSC culture medium (Cyagen, Guangzhou, China). rSCs (Sciencell, America) were cultured in the low glucose–type Dulbecco's modified Eagle medium (DMEM) supplemented with 10% fetal bovine serum (FBS) and 1% penicillin/streptomycin. RBMSCs (Cyagen, Guangzhou, China) were cultured in RBMSC culture medium (Cyagen, Guangzhou, China). RAECs (iCell, Shanghai, China) were cultured in EC Culture Medium (iCell, Shanghai, China).

Establishment of Haversian bone–mimicking scaffold–based cell coculture system

The HBMSC-HUVEC coculture system was established to investigate in vitro osteogenic and angiogenic activities of Haversian bone–mimicking scaffold–based cell coculture system. Scaffolds were prewetted in DMEM for 24 hours within a 24-well plate. Then, the scaffolds were transferred to new wells, and excess liquid on the scaffolds was blotted up by a vacuum pump. A 5-μl aliquot of HUVEC suspension (1×10^6 cells ml^{-1} for cell proliferation assay, and 1×10^7 cells ml^{-1} for cell attachment and differentiation assay) was seeded on the Haversian canals of each scaffold, and 200 μl of HUVEC culture medium was carefully added around each scaffold. Cells were trapped in the Haversian canals because the scaffolds were wet but not immersed in the culture medium. After 1 hour of incubation, the cell-loading scaffolds were washed twice with PBS to remove nonadherent cells, and another 800 μl of HUVEC culture medium was added to immerse the scaffolds. After 12 hours of incubation, the cell-loading scaffolds were transferred to new wells, and excess liquid on the scaffolds was blotted up by a vacuum pump. Then, a 5-μl aliquot of HBMSC suspension (1×10^6 cells ml^{-1} for cell proliferation assay, and 1×10^7 cells ml^{-1} for cell attachment and differentiation assay) was seeded on the cancellous bone structure of each

scaffold, and 200 μl of HBMSC culture medium was carefully added around each scaffold. After 1 hour of incubation, the cell-loading scaffolds were washed twice with PBS and submerged in 1 ml of mixed culture medium (50% HBMSC culture medium and 50% HUVEC culture medium).

The rBMSC-rSC coculture system was established to investigate in vitro neurogenic activities of Haversian bone–mimicking scaffold–based cell coculture system. Three coculture modes with different ratios (rBMSC:rSC = 3:7, rBMSC:rSC = 5:5, and rBMSC:rSC = 7:3) were investigated. Scaffolds were prewetted in DMEM for 24 hours within the 24-well plates. Then, the scaffolds were transferred to new wells, and excess liquid on the scaffolds was blotted up by a vacuum pump. A prorated volume (3.5 μl for the 3:7 group, 2.5 μl for the 5:5 group, and 1.5 μl for the 7:3 group) of rSC suspension (2×10^6 cells ml^{-1} for cell proliferation assay, and 2×10^7 cells ml^{-1} for cell attachment and differentiation assay) was seeded on the Haversian canals of each scaffold, and 200 μl of DMEM (supplemented with 10% FBS and 1% penicillin/streptomycin) was carefully added around each scaffold. After 1 hour of incubation, the cell-loading scaffolds were washed twice with PBS to remove nonadherent cells, and another 800 μl of DMEM (supplemented with 10% FBS and 1% penicillin/streptomycin) was added to immerse the scaffolds. After 12 hours of incubation, the cell-loading scaffolds were transferred to new wells, and excess liquid on the scaffolds was blotted up by a vacuum pump. Then, a variable volume (1.5 μl for the 3:7 group, 2.5 μl for the 5:5 group, and 3.5 μl for the 7:3 group) of rBMSC suspension (2×10^6 cells ml^{-1} for cell proliferation assay, and 2×10^7 cells ml^{-1} for cell attachment and differentiation assay) was seeded on the cancellous bone structure of each scaffold, and 200 μl of rBMSC culture medium was carefully added around each scaffold. After 1 h of incubation, the cell-loading scaffolds were washed twice with PBS and submerged in 1 ml of mixed culture medium (500 μl of rBMSC culture medium and 500 μl of DMEM supplemented with 10% FBS and 1% penicillin/streptomycin).

The RBMSC-RAEC coculture system was established to investigate in vivo osteogenic and angiogenic activities of Haversian bone–mimicking scaffold–based cell coculture system. Scaffolds were prewetted in DMEM for 24 hours within a 24-well plate. Then, the scaffolds were transferred to new wells, and excess liquid on the scaffolds was blotted up by a vacuum pump. A 15-μl aliquot of RAEC suspension (2×10^7 cells ml^{-1}) was seeded on the Haversian canal of each scaffold, and 1 ml of RAEC culture medium was carefully added around each scaffold. Because the scaffolds were wet but not immersed in the culture medium, cells were trapped in the Haversian canals. After 1 hour of incubation, the cell-loading scaffolds were washed twice with PBS to remove nonadherent cells, and another 1 ml of HUVEC culture medium was added to immerse the scaffolds. After 3 days of incubation, the cell-loading scaffolds were transferred to new wells, and excess liquid on the scaffolds was blotted up by a vacuum pump. Then, a 15-μl aliquot of RBMSC suspension (2×10^7 cells ml^{-1}) was seeded on the cancellous bone structure of each scaffold, and 1 ml of RBMSC culture medium was carefully added around each scaffold. After 1 hour of incubation, the cell-loading scaffolds were washed twice with PBS and submerged in 2 ml of mixed culture medium (50% RBMSC culture medium and 50% RAEC culture medium). Cells in the coculture and monoculture groups were seeded simultaneously. The total number of cells was kept consistent in all groups despite culture modes.

Cell proliferation

For cell proliferation of HBMSCs, HUVECs, rBMSCs, and rSCs cultured with the extracts from the Haversian bone–mimicking bioceramic scaffolds on days 1, 3, and 7, four groups of extracts (soaked for 24 hours at 37°C) with different concentrations (scaffold mass to culture medium volume: 0, 200, 100, and 50 mg/ml) were investigated.

For the HBMSC-HUVEC coculture system, five groups of scaffolds with different diameters (D) and numbers (N) of Haversian canals (D = 0.8 mm, N = 8; D = 1.2 mm, N = 8; D = 1.6 mm, N = 8; D = 1.6 mm, N = 4; D = 1.6 mm, N = 2) were investigated. Each group of scaffolds was divided into three groups with different culture modes (HBMSC monoculture, HUVEC monoculture, and HBMSC-HUVEC coculture).

For the rBMSC-rSC coculture system, only one kind of scaffold (D = 1.2 mm, N = 8) was investigated. Scaffolds were divided into five groups with different culture modes (rBMSC monoculture, rSC monoculture, 3:7, 5:5, 7:3).

At each time point (1, 3, 7, and 14 days), cell-loading scaffolds were incubated in 10% CCK-8 solution (Beyotime, China) for 1.5 hours. Absorbance was measured at the 450-nm wavelength with a multifunction microplate reader (SpectraFluor Plus, Tecan, Crailsheim, Germany). Six replicates were used in each group.

Cell attachment

For the HBMSC-HUVEC coculture system, three groups of coculture scaffolds with different diameters of Haversian canals (D = 0.8 mm, N = 8; D = 1.2 mm, N = 8; D = 1.6 mm, N = 8) were investigated. The morphological characteristic of HBMSCs and HUVECs on the coculture scaffolds was observed by CLSM (TCS SP8, Leica). The cytoskeleton of cells was stained with phalloidin (red, Sigma-Aldrich, USA), and the nuclei of cells were stained with DAPI (blue, Sigma-Aldrich, USA). The cell morphology was also characterized by SEM (S-4800, Hitachi, Japan).

For the rBMSC-rSC coculture system, only one group of scaffold (D = 1.2 mm, N = 8) was investigated. Scaffolds were divided into five groups with different ratios of rBMSC to rSC (rBMSC monoculture, rSC monoculture, 3:7, 5:5, 7:3). The cytoskeleton of cells was stained with phalloidin (red), and the nuclei of cells were stained with DAPI (blue) for imaging via CLSM.

Gene expression analysis through RT-PCR

To demonstrate the effect of culture modes to the osteogenic and angiogenic gene expression, scaffolds (D = 1.2 mm, N = 8) with three culture modes (HBMSC monoculture, HUVEC monoculture, and HBMSC-HUVEC coculture) were investigated. To measure the synergistic effect of coculture cells in Haversian bone–mimicking scaffolds, HBMSCs and HUVECs in the coculture group were separated by magnetic beads (Dynabeads, Invitrogen, USA) following the manufacturer's instructions.

To demonstrate the effect of the scaffold parameters to the osteogenic and angiogenic gene expression, five groups of coculture scaffolds with different diameters and numbers of Haversian canals (D = 0.8 mm, N = 8; D = 1.2 mm, N = 8; D = 1.6 mm, N = 8; D = 1.6 mm, N = 4; D = 1.6 mm, N = 2) were investigated. The primer sequences were as follows: glyceraldehyde-3-phosphate dehydrogenase (GAPDH), 5′-ACGGATTTGGTCGTATTGGGCG-3′ (forward) and 5′-CTCCTGGAAGATGGTGATGG-3′ (reverse); ALP, 5′-ACCACCACGAGAGTGAACCA-3′ (forward) and 5′-CGTTGTCTGAGTACCAGTCCC-3′ (reverse); BMP2, 5′-TTCGGCCTGAAACAGAGACC-3′ (forward)

and 5′-CCTGAGTGCCTGCGATACAG-3′ (reverse); Col1, 5′-GAGGGCCAAGACGAAGACATC-3′ (forward) and 5′-CAGATCACGTCATCGCACAAC-3′ (reverse); KDR, 5′-CCCAGGCTCAGCATACAAAAAGAC-3′ (forward) and 5′-CCAGTACAAGTCCCTCTGTCCC-3′ (reverse); eNOS, 5′-TGTCCAACATGCTGCTGGAAATTG-3′ (forward) and 5′-AGGAGGTCTTCTTCCTGGTGATGCC-3′ (reverse); VE-cadherin, 5′-GGCTCAGACATCCACATAACC-3′ (forward) and 5′-CTTACCAGGGCGTTCAGGGAC-3′ (reverse).

To indicate the effect of culture modes to the neurogenic gene expression, scaffolds (D = 1.2 mm, N = 8) with five culture modes (rBMSC monoculture, rSC monoculture, 3:7, 5:5, 7:3) were investigated.

To demonstrate the effect of the scaffold parameters to the neurogenic gene expression, five groups of coculture scaffolds with different diameters and numbers of Haversian canals (D = 0.8 mm, N = 8; D = 1.2 mm, N = 8; D = 1.6 mm, N = 8; D = 1.6 mm, N = 4; D = 1.6 mm, N = 2) were investigated. The primer sequences were as follows: GAPDH, 5′-CTACAGCTTCTTTCTCCTCCTCAG-3′ (forward) and 5′-CTTCTCCATGGTGGTGAAGAC-3′ (reverse); NGF, 5′-GATCGGCGTACAGGCAGAAC-3′ (forward) and 5′-GGCTCGGCACTTGGTCTCAA -3′ (reverse); BDNF, 5′-GTCAAGTGCCTTTGGAGCCT-3′ (forward) and 5′-CTTATGAACCTTTGGAGCCT-3′ (reverse); TrkA, 5′-GTCTGGTGGGTCAGGGACTA-3′ (forward) and 5′-AACGTCCAGGTAACTCGGTG-3′ (reverse); S100, 5′-TTGCCCTCATTGATGTCTTCC-3′ (forward) and 5′-TCTCCATCACTTTGTCCACCAC-3′ (reverse).

Total RNA was extracted by TRIzol reagent (Invitrogen, USA). Complementary DNA (cDNA) was prepared by PrimeScript 1st Strand cDNA synthesis kit (TOYOBO, Japan). RT-PCR was performed using the SYBR Green QPCR Master Mix (TaKaRa, Japan). GAPDH was used as the endogenous control. Gene expression levels were calculated using the $2^{-\Delta\Delta Ct}$ method. Three technical replicates were used in the analysis.

Animal surgery

All animal experiments were implemented in accordance with guidelines approved by the Nanjing Medical University Ethics Committee. A total of 30 male New Zealand white rabbits (2.5 to 3 kg) were used and divided into five groups: blank (no scaffolds), AKT (cell-free akermanite scaffolds), RBMSC (scaffolds cultured with RBMSCs), RAEC (scaffolds cultured with RAECs), and coculture (scaffolds cocultured with RBMSCs and RAECs). All scaffolds used here were designed as cylindrical samples (D = 6 mm and height, 7 mm) with Haversian canals (N = 8 and D = 1 mm), Volkmann canals (N = 3), and cancellous bone structure (meshwork with two cuboids on the same horizontal plane). RAECs (3×10^5) were seeded on each scaffold both in the RAEC group and the coculture group. After incubation for 3 days, 3×10^5 RBMSCs were seeded on each scaffold both in the RBMSC group and the coculture group and were cultured for another 4 days. Then, six samples in each group were implanted in the 6-mm critical-size femoral defects. After 8 weeks, all rabbits were anesthetized, and the abdominal cavity was opened. Then, a 24-gauge cannula was inserted into the abdominal aorta, and 100 ml of heparinized saline (1000 U/ml), 100 ml of 10% neutral buffered formalin solution, and 20 ml of Microfil (Flow Tech, USA) were perfused at 2 ml/min in turn. After being kept for 24 hours at 4°C, the femurs were collected from the rabbits and fixed in 4% paraformaldehyde solution for 48 hours.

Micro-CT analysis

All samples were scanned by micro-CT (SKYSCAN1172, Bruker, Germany) with 8.9-μm resolution. A volume of interest was defined as a cylindrical space (D = 6 mm and height, 7.5 mm). New bone formation was evaluated by BV/TV ratio.

Histological staining

All samples were dehydrated, embedded in methyl methacrylate, and sectioned at 500 μm. After being grinded and polished, the sections were stained with picric acid-acid fuchsin to examine new bone. New blood vessels were shown by Microfil (blue), and the vascular density within the region of defects was analyzed by the software Image-Pro Plus (Media Cybernetics, USA) (*40*).

Statistical analysis

All numerical data were expressed as means ± SD and analyzed in Origin Pro 2015 (OriginLab, USA) by one-way analysis of variance. $^{*}P < 0.05$, $^{**}P < 0.01$, $^{***}P < 0.001$, $^{\$}P < 0.05$, $^{\$\$}P < 0.01$, $^{\$\$\$}P < 0.001$ were considered significantly different.

SUPPLEMENTARY MATERIALS

Supplementary material for this article is available at http://advances.sciencemag.org/cgi/content/full/6/12/eaaz6725/DC1

Fig. S1. Surface roughness of the Haversian bone–mimicking bioceramic scaffolds.
Fig. S2. Compressive modulus of the Haversian bone–mimicking bioceramic scaffolds.
Fig. S3. Flexural strength of the Haversian bone–mimicking bioceramic scaffolds.
Fig. S4. CLSM images of cocultured HBMSCs and HUVECs stained with DAPI and phalloidin.
Fig. S5. Cell proliferation of HBMSCs and HUVECs cultured with the extracts from the Haversian bone–mimicking bioceramic scaffolds on days 1, 3, and 7.
Fig. S6. The osteogenic and angiogenic gene expression of cocultured HBMSC-HUVEC seeded on scaffolds with different diameters and numbers of Haversian canals for 3 days.
Fig. S7. The CLSM images of rBMSCs and rSCs in monoculture group and rBMSC-rSC coculture group with the ratio of rBMSCs to rSCs being 3:7, 5:5, and 7:3 stained with DAPI (blue) and phalloidin (red).
Fig. S8. Cell proliferation of rBMSCs and rSCs cultured with the extracts from the Haversian bone–mimicking bioceramic scaffolds on days 1, 3, and 7.
Fig. S9. The neurogenic gene expression of cocultured rBMSC-rSC seeded on scaffolds with different diameters and numbers of Haversian canals for 3 days.
Fig. S10. New bone formation evaluated by histological analysis.
Movie S1. The bottom-up printing process to fabricate Haversian bone–mimicking scaffolds for multicellular delivery.
Movie S2. The bottom-up printing process to fabricate Haversian bone–mimicking scaffolds with different numbers of Haversian canals for mechanical and porosity tests.
Movie S3. The bottom-up printing process to fabricate Haversian bone–mimicking scaffolds with different diameters of Haversian canals for mechanical and porosity tests.
Movie S4. The bottom-up printing process to fabricate Haversian bone–mimicking scaffolds with different numbers of Volkmann canals for mechanical and porosity tests.

REFERENCES AND NOTES

1. Y. Liu, D. Luo, T. Wang, Hierarchical structures of bone and bioinspired bone tissue engineering. *Small* **12**, 4611–4632 (2016).
2. M. A. Fernandez-Yague, S. A. Abbah, L. McNamara, D. I. Zeugolis, A. Pandit, M. J. Biggs, Biomimetic approaches in bone tissue engineering: Integrating biological and physicomechanical strategies. *Adv. Drug Deliv. Rev.* **84**, 1–29 (2015).
3. O. A. Tertuliano, J. R. Greer, The nanocomposite nature of bone drives its strength and damage resistance. *Nat. Mater.* **15**, 1195–1202 (2016).
4. B. Langdahl, S. Ferrari, D. W. Dempster, Bone modeling and remodeling: Potential as therapeutic targets for the treatment of osteoporosis. *Ther. Adv. Musculoskelet. Dis.* **8**, 225–235 (2016).
5. A. Marrella, T. Y. Lee, D. H. Lee, S. Karuthedom, D. Syla, A. Chawla, A. Khademhosseini, H. L. Jang, Engineering vascularized and innervated bone biomaterials for improved skeletal tissue regeneration. *Mater. Today* **21**, 362–376 (2018).
6. U. G. K. Wegst, H. Bai, E. Saiz, A. P. Tomsia, R. O. Ritchie, Bioinspired structural materials. *Nat. Mater.* **14**, 23–36 (2015).
7. M. Nippier, E. D. Lemma, S. Bertels, E. Blasco, C. Barner-Kowollik, M. Wegener, M. Bastmeyer, 3D scaffolds to study basic cell biology. *Adv. Mater.* **31**, 1808110 (2019).

8. Q. F. Cheng, C. J. Huang, A. P. Tomsia, Freeze casting for assembling bioinspired structural materials. *Adv. Mater.* **29**, 1703155 (2017).
9. J. Xue, C. Feng, L. Xia, D. Zhai, B. Ma, X. Wang, B. Fang, J. Chang, C. Wu, Assembly preparation of multilayered biomaterials with high mechanical strength and bone-forming bioactivity. *Chem. Mater.* **30**, 4646–4657 (2018).
10. Y. Yang, X. J. Li, M. Chu, H. F. Sun, J. Jin, K. H. Yu, Q. M. Wang, Q. F. Zhou, Y. Chen, Electrically assisted 3D printing of nacre-inspired structures with self-sensing capability. *Sci. Adv.* **5**, eaau9490 (2019).
11. A. Velasco-Hogan, J. Xu, M. A. Meyers, Additive manufacturing as a method to design and optimize bioinspired structures. *Adv. Mater.* **30**, 1800940 (2018).
12. C. Feng, W. Zhang, C. Deng, G. Li, J. Chang, Z. Zhang, X. Jiang, C. Wu, 3D printing of lotus root-like biomimetic materials for cell delivery and tissue regeneration. *Adv. Sci.* **4**, 1700401 (2017).
13. T. Li, D. Zhai, B. Ma, J. Xue, P. Zhao, J. Chang, M. Gelinsky, C. Wu, 3D printing of hot dog-like biomaterials with hierarchical architecture and distinct bioactivity. *Adv. Sci.* 1901146 (2019).
14. A. Lee, A. R. Hudson, D. J. Shiwarski, J. W. Tashman, T. J. Hinton, S. Yerneni, J. M. Bliley, P. G. Campbell, A. W. Feinberg, 3D bioprinting of collagen to rebuild components of the human heart. *Science* **365**, 482–487 (2019).
15. B. Grigoryan, S. J. Paulsen, D. C. Corbett, D. W. Sazer, C. L. Fortin, A. J. Zaita, P. T. Greenfield, N. J. Calafat, J. P. Gounley, A. H. Ta, F. Johansson, A. Randles, J. E. Rosenkrantz, J. D. Louis-Rosenberg, P. A. Galie, K. R. Stevens, J. S. Miller, Multivascular networks and functional intravascular topologies within biocompatible hydrogels. *Science* **364**, 458–464 (2019).
16. X. Zhang, J. Li, P. Ye, G. Gao, K. Hubbell, X. Cui, Coculture of mesenchymal stem cells and endothelial cells enhances host tissue integration and epidermis maturation through AKT activation in gelatin methacryloyl hydrogel-based skin model. *Acta Biomater.* **59**, 317–326 (2017).
17. X. N. Chen, A. Ergun, H. Gevgilili, S. Ozkan, D. M. Kalyon, H. J. Wang, Shell-core bi-layered scaffolds for engineering of vascularized osteon-like structures. *Biomaterials* **34**, 8203–8212 (2013).
18. Y. Zuo, X. Liu, D. Wei, J. Sun, W. Xiao, H. Zhao, L. Guo, Q. Wei, H. Fan, X. Zhang, Photo-cross-linkable methacrylated gelatin and hydroxyapatite hybrid hydrogel for modularly engineering biomimetic osteon. *ACS Appl. Mater. Interfaces* **7**, 10386–10394 (2015).
19. C. Piard, H. Baker, T. Kamalitdinov, J. Fisher, Bioprinted osteon-like scaffolds enhance in vivo neovascularization. *Biofabrication* **11**, 025013 (2019).
20. S. H. Kim, Y. K. Yeon, J. M. Lee, J. R. Chao, Y. J. Lee, Y. B. Seo, M. T. Sultan, O. J. Lee, J. S. Lee, S.-i. Yoon, I.-S. Hong, G. Khang, S. J. Lee, J. J. Yoo, C. H. Park, Precisely printable and biocompatible silk fibroin bioink for digital light processing 3D printing. *Nat. Commun.* **9**, 1620 (2018).
21. J. A. Robles-Linares, E. Ramírez-Cedillo, H. R. Siller, C. A. Rodriguez, J. Israel Martínez-López, Parametric modeling of biomimetic cortical bone microstructure for additive manufacturing. *Materials* **12**, E913 (2019).
22. B. Kang, J. Shin, H.-J. Park, C. Rhyou, D. Kang, S.-J. Lee, Y.-s. Yoon, S.-W. Cho, H. Lee, High-resolution acoustophoretic 3D cell patterning to construct functional collateral cylindroids for ischemia therapy. *Nat. Commun.* **9**, 5402 (2018).
23. G. Huang, F. Li, X. Zhao, Y. Ma, Y. Li, M. Lin, G. Jin, T. Lu, G. Genin, F. Xu, Functional and biomimetic materials for engineering of the three-dimensional cell microenvironment. *Chem. Rev.* **117**, 12764–12850 (2017).
24. D.-C. Cho, H. J. Brennan, R. W. Johnson, I. J. Poulton, J. H. Gooi, B. A. Tonkin, N. E. McGregor, E. C. Walker, D. J. Handelsman, T. J. Martin, N. A. Sims, Bone corticalization requires local SOCS3 activity and is promoted by androgen action via interleukin-6. *Nat. Commun.* **8**, 806 (2017).
25. J. N. Farr, S. Khosla, Skeletal changes through the lifespan—From growth to senescence. *Nat. Rev. Endocrinol.* **11**, 513–521 (2015).
26. E. A. Zimmermann, R. O. Ritchie, Bone as a structural material. *Adv. Healthc. Mater.* **4**, 1287–1304 (2015).
27. R. A. Perez, S.-J. Choi, C.-M. Han, J.-J. Kim, H. Shim, K. W. Leong, H.-W. Kim, Biomaterials control of pluripotent stem cell fate for regenerative therapy. *Prog. Mater. Sci.* **82**, 234–293 (2016).
28. P. Samal, C. van Blitterswijk, R. Truckenmuller, S. Giselbrecht, Grow with the flow: When morphogenesis meets microfluidics. *Adv. Mater.* **31**, 1805764 (2019).
29. Y. Deng, C. Jiang, C. Li, T. Li, M. Peng, J. Wang, K. Dai, 3D printed scaffolds of calcium silicateβ-TCP synergize with co-cultured endothelial and stromal cells to promote vascularization and bone formation. *Sci. Rep.* **7**, 5588 (2017).
30. Y. Kang, S. Kim, M. Fahrenholtz, A. Khademhosseini, Y. Yang, Osteogenic and angiogenic potentials of monocultured and co-cultured human-bone-marrow-derived mesenchymal stem cells and human-umbilical-vein endothelial cells on three-dimensional porous beta-tricalcium phosphate scaffold. *Acta Biomater.* **9**, 4906–4915 (2013).
31. T. Menge, M. Gerber, K. Wataha, W. Reid, S. Guha, C. S. Cox, P. Dash, M. S. Reitz Jr., A. Y. Khakoo, S. Pati, Human mesenchymal stem cells inhibit endothelial proliferation and angiogenesis via cell–cell contact through modulation of the VE-Cadherin/β-catenin signaling pathway. *Stem Cells Dev.* **22**, 148–157 (2013).
32. A. B. Faia-Torres, M. Charnley, T. Goren, S. Guimond-Lischer, M. Rottmar, K. Maniura-Weber, N. D. Spencer, R. L. Reis, M. Textor, N. M. Neves, Osteogenic differentiation of human mesenchymal stem cells in the absence of osteogenic supplements: A surface-roughness gradient study. *Acta Biomater.* **28**, 64–75 (2015).
33. J. Chen, L. Deng, C. Porter, G. Alexander, D. Patel, J. Vines, X. X. Zhang, D. Chasteen-Boyd, H.-J. Sung, Y.-P. Li, A. Javed, S. Gilbert, K. Cheon, H.-W. Jun, Angiogenic and osteogenic synergy of human mesenchymal stem cells and human umbilical vein endothelial cells cocultured on a nanomatrix. *Sci. Rep.* **8**, 15749 (2018).
34. H. Chen, B. Hu, X. Lv, S. Zhu, G. Zhen, M. Wan, A. Jain, B. Gao, Y. Chai, M. Yang, X. Wang, R. Deng, L. Wang, Y. Cao, S. Ni, S. Liu, W. Yuan, H. Chen, X. Dong, Y. Guan, H. Yang, X. Cao, Prostaglandin E2 mediates sensory nerve regulation of bone homeostasis. *Nat. Commun.* **10**, 181 (2019).
35. J. Xue, J. Yang, D. M. O'Connor, C. Zhu, D. Huo, N. M. Boulis, Y. Xia, Differentiation of bone marrow stem cells into schwann cells for the promotion of neurite outgrowth on electrospun fibers. *ACS Appl. Mater. Interfaces* **9**, 12299–12310 (2017).
36. J. Wang, F. Ding, Y. Gu, J. Liu, X. S. Gu, Bone marrow mesenchymal stem cells promote cell proliferation and neurotrophic function of Schwann cells in vitro and in vivo. *Brain Res.* **1262**, 7–15 (2009).
37. P. Carmeliet, M. Tessier-Lavigne, Common mechanisms of nerve and blood vessel wiring. *Nature* **436**, 193–200 (2005).
38. H.-W. Kang, S. J. Lee, I. K. Ko, C. Kengla, J. J. Yoo, A. Atala, A 3D bioprinting system to produce human-scale tissue constructs with structural integrity. *Nat. Biotechnol.* **34**, 312–319 (2016).
39. H. Li, R. Daculsi, M. Grellier, R. Bareille, C. Bourget, J. Amedee, Role of neural-cadherin in early osteoblastic differentiation of human bone marrow stromal cells cocultured with human umbilical vein endothelial cells. *Am. J. Physiol. Cell Physiol.* **299**, C422–C430 (2010).
40. L. Wang, L.-x. Zhu, Z. Wang, A.-j. Lou, Y.-x. Yang, Y. Guo, S. Liu, C. Zhang, Z. Zhang, H.-s. Hu, B. Yang, P. Zhang, H.-w. Ouyang, Z.-y. Zhang, Development of a centrally vascularized tissue engineering bone graft with the unique core-shell composite structure for large femoral bone defect treatment. *Biomaterials* **175**, 44–60 (2018).

Acknowledgments

Funding: This work was supported by the National Key Research and Development Program of China (2018YFC1105201), the National Natural Science Foundation of China (81771989 and 51761135103), the Innovation Cross Team of the Chinese Academy of Sciences (JCTD-2018-13), the STS Program of the Chinese Academy of Sciences (KFJ-STS-QYZD-092), and the Science and Technology Commission of Shanghai Municipality (17540712300). **Author contributions:** M.Z. and C.W. conceived the project. M.Z., C.F., and L.W. performed the 3D printing process. M.Z. and X.W. performed materials preparation and characterization. M.Z., R.L., and C.D. performed in vitro experiments. M.Z., R.L., H.Z., J.M., and C.Q. performed animal surgeries. M.Z. collected and analyzed all the data. M.Z. wrote the manuscript, and all authors discussed the manuscript. **Competing interests:** The authors declare that they have no competing interests. **Data and materials availability:** All data needed to evaluate the conclusions in the paper are present in the paper and/or the Supplementary Materials. Additional data related to this paper may be requested from the authors.

Submitted 29 September 2019
Accepted 23 December 2019
Published 20 March 2020
10.1126/sciadv.aaz6725

Citation: M. Zhang, R. Lin, X. Wang, J. Xue, C. Deng, C. Feng, H. Zhuang, J. Ma, C. Qin, L. Wan, J. Chang, C. Wu, 3D printing of Haversian bone–mimicking scaffolds for multicellular delivery in bone regeneration. *Sci. Adv.* **6**, eaaz6725 (2020).